Dependence of 29Si NMR chemical shielding properties of precursor silicate species, Q0 on its local structure at the pre-nucleation stages of zeolite synthesis – A DFT based comput...

ARTICLE *in* MICROPOROUS AND MESOPOROUS MATERIALS · JULY 2013

Impact Factor: 3.45 · DOI: 10.1016/j.micromeso.2009.02.022

2 AUTHORS, INCLUDING:

Kaliaperumal Selvaraj
CSIR - National Chemical Laboratory, Pune
31 PUBLICATIONS **219** CITATIONS

Microporous and Mesoporous Materials 122 (2009) 105–113

Contents lists available at ScienceDirect

Microporous and Mesoporous Materials

journal homepage: www.elsevier.com/locate/micromeso

Dependence of ^{29}Si NMR chemical shielding properties of precursor silicate species, Q^0 on its local structure at the pre-nucleation stages of zeolite synthesis – A DFT based computational correlation

Kaliaperumal Selvaraj *, Reshmi Kurian

Catalysis Division, National Chemical Laboratory, Dr. Homi Bhabha Road, Pashan, Pune, Maharashtra 411008, India

ARTICLE INFO

Article history:
Received 19 August 2006
Received in revised form 7 February 2009
Accepted 10 February 2009
Available online 20 February 2009

Keywords:
Zeolite
Synthesis
Q^0 silicate species
Ab initio method
Density functional theory (DFT)
^{29}Si NMR chemical shift
NBO analysis
Perturbation theory
Electron density

ABSTRACT

The exploration for new zeolite structures with tailored framework architectures for enhanced catalytic applications requires the knowledge about their nucleation and crystallization at molecular level. Nuclear magnetic resonance (NMR) is one of the most widely tried techniques to understand this. However, by NMR, it is difficult to accurately assign the molecular level precursor silicate structures at the pre-nucleation stages of zeolite synthesis. Hence, understanding the chemical shielding of such precursor molecules using quantum mechanical (QM) computations is extremely useful. Alkali is a fundamental component in the alkali based hydrothermal zeolite synthesis and its nature plays a major role. In the present report, we attempt to understand the differences in the local structure of the primary building block such as $Si(OH)_4$ (Q^0 silicate species) due to the associated alkali and their influence on NMR chemical shielding properties. Present work reports the calculation of ^{29}Si NMR isotropic chemical shifts of Q^0 species with different cations such as Na, K and Ca using density functional theory (DFT). Results of natural bonding orbital (NBO) analysis, Perturbation theory energy analysis and electron density iso-surfaces were employed to obtain a deeper insight about their influence on the chemical shielding and on zeolite synthesis.

1. Introduction

Synthesis of crystalline porous aluminosilicates remains as one of the most promising area in heterogeneous catalysis related research for the past several decades. A number of innovative recipes with novel approaches have been reported under the theme of hydrothermal synthesis for new zeolite structures with many striking features [1–9]. Nevertheless the hydrothermal synthesis has been poorly understood in terms of the fundamental interactions between the molecules present in the synthesis gel mixture and especially the actual role of them in the process of zeolite crystallization [10–14]. A typical zeolite synthesis method involves various steps such as hydrolysis of sources, gel formation and condensation of the precursors or crystallization. Hydrolysis is the process of breaking of larger molecular units of the silicon and aluminum sources into the primary building blocks such as orthosilicic acid, $Si(OH)_4$, prominently known as the Q^0 species in silicate chemistry. This is generally carried out at elevated pH (>10). Alkali metal hydroxides are used as 'mineralizing agents'. After gel formation, the primary building units condense together to form oligomers, known as Q^n species (where $n = 1–4$) and finally into the large periodic crystals with various structural features depending on the templating molecules used during the synthesis. The alkali metal atoms often prefer to remain as exchangeable extra-framework charge compensating cations. Thus, each component in the zeolite synthesis mixture influences the final structure. For instance, the alkali cations have been understood to be one of the major influencing factors [15]. Although various alkali elements have been considered in this regard, sodium has been the most profoundly used alkali cation in zeolite synthesis. It is due to the unambiguous reason of being able to maintain a better alkaline pH which brings about the easy mineralization of the silicon and aluminum sources [16a–d]. Apart from sodium, alkali elements such as potassium and lithium have seldom been tried [17]. The process of crystallization and its kinetics were observed to be different with different alkali cations [18,19]. It was reported that cations influence the crystallite sizes and even the morphology of silicate structures [20,21]. However, the other crucial roles of the cation (in alkali hydroxide) in zeolite crystallization beyond as mineralizing agent have been poorly understood. In principal, the predominant presence of silicate precursor species such as the hydrolyzed orthosilicic acid (Q^0), $Si(OH)_4$ in the pre-nucleation stage of synthesis mixture has been more or less qualitatively observed by various techniques such as nuclear magnetic resonance (NMR) and reported [29]. Hence, the influence of cations on the crystallization is highly associated with the reactive response of these primary building blocks to the presence of an alkali. One

* Corresponding author. Tel.: +91 20 25 90 22 62; fax: +91 20 25 90 26 33.
E-mail addresses: k.selvaraj@ncl.res.in, kselva@gmail.com (K. Selvaraj).

1387-1811/$ - see front matter © 2009 Elsevier Inc. All rights reserved.
doi:10.1016/j.micromeso.2009.02.022

plausible and direct lead to understand this could be through a close observation of the changes in the local structure of the precursor silicate molecular species with reference to an associated alkali cation. Hence, the present investigation was intended to observe such changes at the most crucial and the very origin stage of local domain such as in a single orthosilicic acid molecule, $Si(OH)_4$ or the 'Q^0' species. Hence, the knowledge about the local molecular environment of the precursor silicate Q^0 species is the key to design new porous structures. However, it is yet a challenge to understand them precisely.

By and large, the techniques such as powder X-ray diffraction (PXRD) and solid-state nuclear magnetic resonance (NMR) are the two major characterization tools widely used to understand the crystallization of zeolites and its kinetics. However, due to their inherent limitations, it is ineffective in meeting such objectives. For instance, PXRD is limited to the investigations of only the larger crystallites which are in principle known as 'crystalline' matter and hence using XRD to understand such a diminutive local domain such as a Q^0 species is inapprehensible. Solid state NMR, on the other hand, is limited due to the fact that the information inferred is principally an average picture of dynamically changing local structural parameters with in a finite time domain that is larger than that of the intra-and inter-molecular interactions between the various silicate precursor species during the synthesis. Moreover, the precise assignment of ^{29}Si NMR chemical shifts (δ) for Q^0 species in the presence of different cations in experiments has always been a challenge.

The actual NMR chemical shielding of a nucleus is directly based on the effective electron density around it. The information about the changes in the electron density due to different cations can be correlated to the changes in the local structure. Hence, if the changes in the chemical shielding around Si nucleus can be computed, understanding the corresponding local structure of Q^0 species is much easier. This forms the basis for our study on local structure using the theoretically computed chemical shift (δ) values. Further, it may be noted that the computed δ value for a Q^0 species gives the direct and more accurate information about the local environment unlike what is observed in experimental NMR techniques as averaged overall information from millions of such species of different geometries. Thus, the understanding about the molecular level structural aspects of Q^0 species becomes easier. It may be noted here that contrastingly the interactions of cations on the large periodic structures of zeolites have been studied considerably and reported [16b–d]. So, it is reiterated here that our present investigation essentially focuses only on the precursor silicate monomeric unit, $Si(OH)_4$, the Q^0 species.

We have used density functional theory (DFT) based *ab initio* computational methods to optimize and compute the NMR δ values of Q^0 silicate precursor models. Reports are observed on the *ab initio* calculations of NMR chemical shift values of various crystalline dense phase silicates using various theory levels but in the general context of three dimensional solid silicates [22]. However, rarely few works have been reported regarding that of the hydrothermal synthesis of zeolite [23]. To the best of our knowledge there are no reports available on the changes in the local structure of Q^0 species due to the attached alkali cation and their influences on the NMR chemical shift values. In that way, the present investigation, for the first time, presents an insight about the influence of cation on the local chemical environment of Q^0 species which is the prime pre-nucleation Si species. To understand the characteristic influence of the alkali, cations such as potassium and calcium have been considered and compared with sodium, the prime alkali mainly used in zeolite synthesis. These alkali elements are substituted in the Q^0 species in one of the positions of the four protons. However, as a case of example, elaborate quantitative studies have been carried out with Q^0 with potassium apart from that with sodium. As potassium is the next most widely used alkali in zeolite synthesis next to sodium, the scope of the major findings in the present work is mainly pointed towards them. The attributions to their respective influences on Q^0 silicate precursor are evaluated here. Although the scope of present study is essentially focused mainly on $Si(OH)_4$, the Q^0 species, as a case of exception, dimer (Q^1) species with two Si atoms that are bridged by an oxygen has also been studied for understanding the long range influences of the cation.

2. Computational methodology

2.1. Density functional theory calculations

All *ab initio* theoretical calculations were performed using standard package of Gaussian98 [24]. Initially the geometry of $Si(OH)_4$ tetrahedron model was optimized using self consistency field (SCF) algorithm as implemented in Gaussian98 at Hartree–Fock (HF) level of theory with a 6-31G basis set. This model was then used for substituting cations such as Na^+, K^+, etc., at the position of the terminal H atoms. The alkali metal (M^+) substituted Q^0 models were further optimized at DFT level with the HF self-interaction corrected, hybrid B3LYP functional with split valence basis set along with polarization and diffuse parameters viz., 6-311G+ (2d,p).

It may be noted that the Q^0 model substituted with Na^+ cation would be referred as Na–Q^0, that substituted with K^+ as K–Q^0 and that substituted with Ca^{2+} as Ca–Q^0 (in general, M–Q^0 where M = Na/K/Ca) henceforth in this text; similarly, the geometrical parameters such as bond distances as O–M, bond angles as Si–O–M and dihedral angles as M–O–Si–O, etc., It may also be noted that the nomenclature of atom label numbers given in subscript to the element name (eg., 'Si_3' indicates the Si atom bearing the label 3 as seen in Na–Q^0 model in Fig. 1a) will be followed through out this text.

2.2. The NMR chemical shielding calculations

The ^{29}Si NMR δ values of the optimized geometries were calculated using the Gauge-independent atomic orbital (GIAO) method [25] as implemented in the general Gaussian98 program. The GIAO based NMR δ calculations were performed at DFT level with B3LYP functional and with split valence 6-311G+ (2d,p) basis with polarization and diffuse parameters. The calculated isotropic ^{29}Si NMR δ values were later corrected with that of standard tetramethylsilane (TMS).

2.3. Natural bonding orbital calculations

Natural Bonding Orbital (NBO) analysis [26] is based on a method for optimally transforming a given wave function into localized form, corresponding to the one-center (''lone pair'') and two-center (''bond'') elements of the chemist's Lewis structure picture [27].

As the NBOs are obtained as a local block eigen functions of the one-electron matrix, they have optimal convergence properties for describing the electron density. However, on the process of the obtaining the NBOs, the set of high-occupancy NBOs, each taken doubly occupied is said to represent the ''natural Lewis structure'' of the molecule and the delocalization effects appear as weak departures from this idealized localized picture. However, during the present study it is realized that they proved to be highly sensitive in revealing the extent of delocalization and that these changes seem to have significant correlation with their chemical shielding properties. However, the discussions based on the localized picture of electron density through their occupancies are also verified with the electron density iso-surfaces generated for the overall molecular system of the Q^0 species.

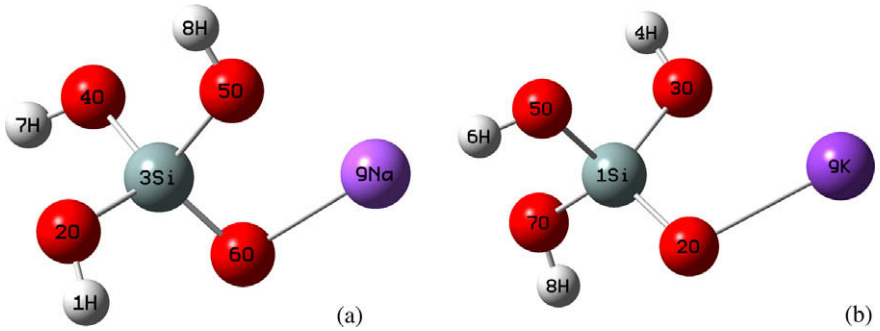

Fig. 1a and 1b. Optimized monomeric silicate Q^0 model with (a) Na and (b) K cations used for GIAO calculations.

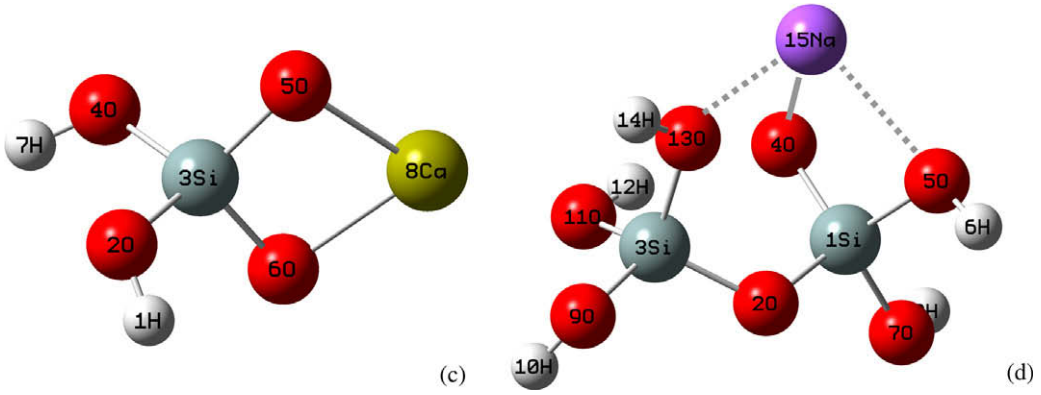

Fig. 1c and 1d. Optimized monomeric silicate Q^0 model with Ca (c) and dimeric silicate model Q^1 with Na (d) cation used for GIAO calculations.

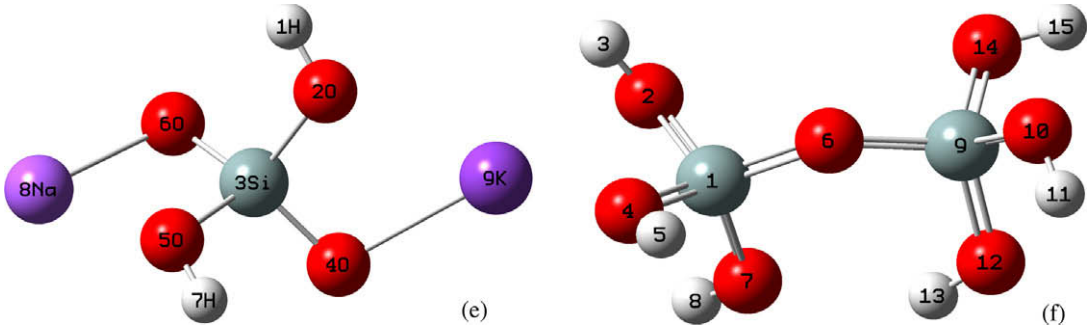

Fig. 1e and 1f. Optimized monomeric silicate Q^0 model with Na and K (e) used for GIAO and electron density calculations and optimized Q^1 dimer model (f) used for studying the effects on remote Si atom.

2.4. Perturbation theory energy analysis

The energetics associated with all possible interactions between 'filled' (donor) Lewis-type NBOs and 'empty' (acceptor) non-Lewis NBOs are estimated using a second order perturbation theory based analysis. Since these interactions lead to loss of occupancy from the localized NBOs of the idealized Lewis structure into the 'empty' non-Lewis orbitals (and thus, to departures from the idealized Lewis structure description), they are also referred to as 'delocalization' corrections to the zeroth-order natural Lewis structure. For each donor NBO (i) and acceptor NBO (j), the stabilization energy $E(2)$ associated with delocalization ("2e-stabilization") $i \rightarrow j$ is estimated as

$$E(2) = \Delta E_{ij} = q_i(F(i,j)^2)/(\epsilon_j - \epsilon_i)$$

where q_i is the donor orbital occupancy, ε_i, ε_j are diagonal elements (orbital energies) and $F(i,j)$ is the off-diagonal NBO Fock matrix element. It may be noted that the entries in this analysis are limited to only those interactions whose interaction energy exceeds a default threshold of 0.5 kcal/mol.

During the present investigation, extensive natural bonding orbital (NBO) analyses and the second order perturbation theory based energy calculations were performed on different M–Q^0 models generated during the geometrical parameter variations. These calculations were performed using the standard NBO algorithm [28] as implemented in the regular Gaussian98 [24] package.

3. Results and discussion

Figs. 1(a–c) shows the optimized geometries of Q^0 species substituted with Na, K and Ca. The geometrical parameters and the calculated ^{29}Si NMR δ values of them are as given in Table 1. The Si–O–M bond angle and O–M bond length for each M–Q^0 is different as seen in the table, where as the dihedral angles O–Si–O–M

Table 1
Optimized geometries of alkali substituted Q^0 species.

Parameters	Na–Q^0 (Ref. Fig. 1a)	K–Q^0 (Ref. Fig. 1b)	Ca–Q^0 [d] (Ref. Fig. 1c)
Si–O–M bond angle (°)	97.180	103.310	91.560 (Si_3–O_6–Ca_8), 92.183 (Si_3–O_5–Ca_8)
O–M Bond length (Å)	2.111	2.402	2.067 (O_6–Ca_8), 2.058 (O_5–Ca_8)
O_n–M non-bonded distance[a] (Å)	2.274	2.657	2.685 (O_4–O_5), 2.789 (O_4–O_6)
Dihedral angle with next oxygen atom (°)	−5.682 (O_5–Si_3–O_6–Na_9)	7.046 (O_3–Si_1–O_2–K_9)	−118.633 (Ca_8–O_5–Si_3–O_4), 123.234 (Ca_8–O_5–Si_3–O_2)
van der Waal radius (r_{vdW}) of M (Å)	1.960	2.350	–
Overlap free distance[b] {$r_{vdW}M^+ + (r_{vdW}\ O^- = 0.74)$} (Å)	2.700	3.090	–
Critical radius overlap distance[c] (Å)	0.590	0.689	–
^{29}Si NMR chemical shift (δ) (−ppm)	71.314	75.038	78.656

[a] O_n–M^+ non-bonded distance is the distance of the cation from the next neighboring hydroxyl bridging oxygen atom (for Na monomer $n = 5$ and for K monomer $n = 3$; refer Fig. 1).
[b] Calculated distance by summation of van der Waals radii of O and M without any overlapping.
[c] Calculated radii overlap distance by deducing the calculated equilibrium bond length of O–M from the sum of van der Waals radii of O and of M.
[d] Ca^{2+} cation bonds with two oxygens (O_6 and O_5) and hence the overlap information has not been considered/provided.

for Na and K are relatively closer and that of Ca is different. It may be noted Ca, being divalent bonds with two adjacent oxygen atoms unlike Na and K as seen in Figs. 1(a–c). The effect of local geometrical structure on NMR chemical shielding around Si nucleus was studied by monitoring the computed δ values while varying few of the geometric parameters periodically as described later in the text.

The ^{29}Si NMR isotropic chemical shifts (δ) calculated were corrected to the calculated standard δ value of tetramethylsilane (TMS) and are given in Table 1. The calculated NMR δ for Q^0 species with Na is −71.31 ppm, for that with K is −75.04 and for that of Ca is −78.656. The experimentally observed δ value for alkali substituted Q^0 is −71.3 ppm [29]. Thus, the calculated δ values have been found to be with in the close range of the experimental values demonstrating the validity of optimized M–Q^0 model with respect to the realistic conditions. However, in realistic situations the geometry undergoes numerous dynamic variations due to intra- and inter-molecular vibrations with in an infinitesimally short span of time and hence it is important to understand the influence of the cation on the local structure. Here we monitor this through the changes in the molecular properties of Q^0 such as ^{29}Si NMR δ values which is an indicator of the electronic environment immediately around the central Si atom.

To study this, the geometric parameters such as bond length and bond angle of the optimized geometries of Na, K and Ca substituted Q^0 were varied periodically above and below their equilibrium values. In particular, the results of O–M bond lengths and Si–O–M bond angles variations as they are directly linked with the cations are elaborated here. With reference to the nomenclature as shown in Figs. 1a–c, the bond lengths such as O_6–Na_9 and O_2–K_9 and similarly the bond angles such as Si_3–O_6–Na_9 of the Na–Q^0 and that of Si_1–O_2–K_9 of K–Q^0 were varied at regular intervals and their corresponding δ values were calculated. Plots provided in Figs. 2 and 3 show the changing trends of δ values due to variations in O–K and O–Na bond lengths, respectively. K shows a linear variation where as the Na shows an exponential decay of the δ values during the bond length variation. Plots provided in Figs. 3b and c show the changing trends of δ values due to variations in O–Ca and Si–O–Ca bond angles, respectively.

To understand the effect of such variation on the chemical shielding of a remote Si atom, a dimer model as shown in Fig. 1f was used. As the purpose was to understand the only the trends of such variations, for computational simplicity, the optimization and GIAO calculations were performed at a level of HF/6-31G-d (only for this case). The δ values corrected for the standard TMS were calculated and plotted (Fig. 5a) against the varying lengths around the equilibrium value of the terminal O_{14}–H_{15} bond. The changes in the δ of Si_9, which is the vicinal Si atom to the O–H bond shows a non-linear variation while that of Si_1, the remote Si atom

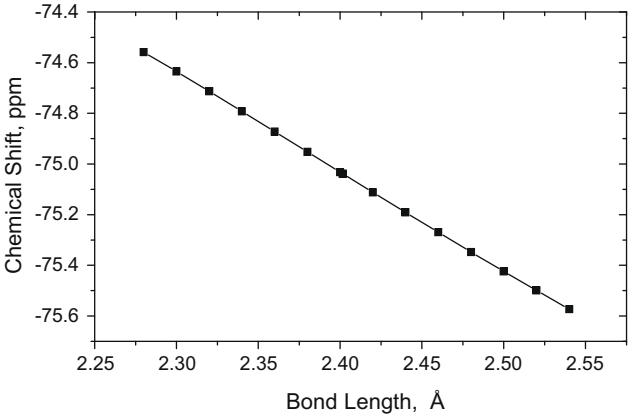

Fig. 2. ^{29}Si NMR δ vs O–K bond length variation on K–Q^0 model.

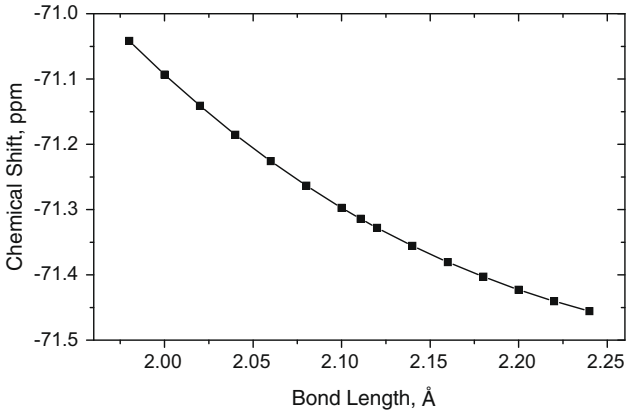

Fig. 3a. ^{29}Si NMR δ vs O–Na bond length variation on Na–Q^0 model.

shows a linear trend, confirming the influence is predominantly localized and limited with the vicinal Si atom.

Further, the bond angle of Si–O–M^+ was varied and their respective δ values were calculated. Fig. 4 shows the multiple plots of δ vs the bond angles of Si–O–K and Si–O–Na. It is interesting to note that the curve for Na is showing a relatively flat and almost linear trend where as the one for K shows a harmonic variation around the minimum energy geometry (equilibrium Si–O–K bond angle = 103.3 degrees). The distinct trend for each cation demonstrates the characteristic interaction of each cation with the Q^0 species and that they are disparate. The differences in trends of δ values compared with the non-bonded distance (as shown in

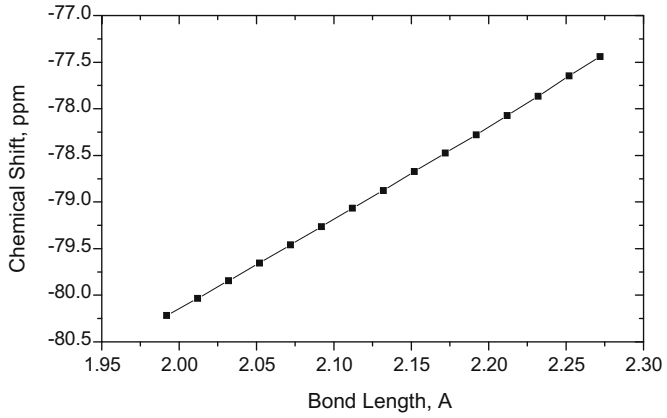

Fig. 3b. ^{29}Si NMR δ vs O–Ca bond length variation on Ca–Q^0 model.

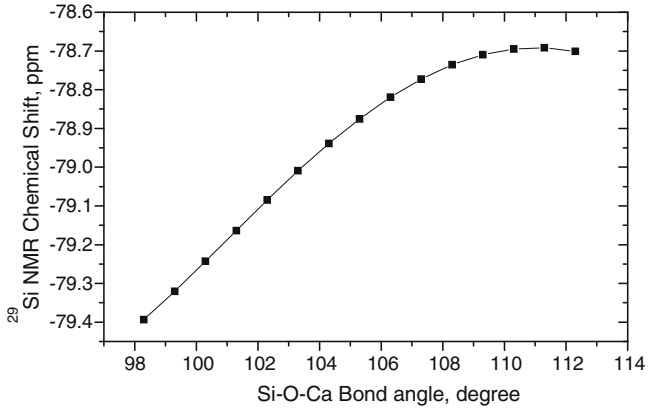

Fig. 3c. ^{29}Si NMR δ vs Si–O–Ca bond angle variation on Ca–Q^0 model.

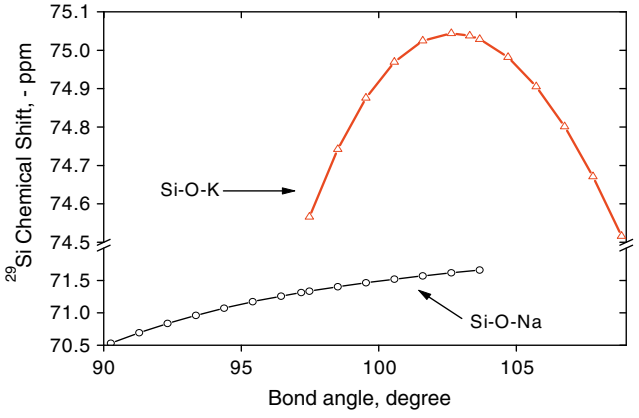

Fig. 4. Plot of ^{29}Si NMR δ of monomeric species with different cations Na^+ and K^+ as a function of the Si–O–M angle.

Table 1) suggest the possibility of characteristic intra-molecular interaction of the alkali cation M with its neighboring bridging oxygen atom. A deeper understanding of the possible reasons for such differences is of great importance to reveal the sensitivity of the local structure of Q^0 species with respect to the alkali cation attached with. As a specific illustrative case, the nature of interaction between the cations such as Na and K and the Q^0 was studied in depth. However, as the interaction of the divalent Ca cation is not limited to a single electronegative centre in the Q^0 species (Fig. 1c), the Ca case is entirely different from mono-valent cations. Hence, the further detailed study was restricted with the Q^0 species substituted with similar mono-valent cations, such as Na and K and not to that with Ca.

As the NMR chemical shift is basically a tensor property of the chemical shielding around Si atom, the Mulliken charge which is an indicator of the electron density around Si atom was measured for all the geometries considered through out the variation of bond angle. The plot of the Mulliken charges on the Si atom vs the Si–O–M bond length as shown in Fig. 5b reveals the correlation. The similarity among the two trends as observed in Figs. 4 and 5b is clearly elucidating that the local structure around the Si atom is very sensitive to the cation attached to it and that the cation has its own characteristic influence in the effective electronic environment around Si (Fig. 6).

One of the simpler ways to analyze the different influence between cations Na and K, is through the charge to radius ratio of the cations. As shown in Table 1, the van der Waal's radius of K is 1.12 times larger than that of the Na where as both are univalent cations bearing the similar formal charge. Due to its smaller radius for the charge, Na has better chances of influencing the electrons and their density than K. Since oxygen is bridging them with the Si atom, the critical radii overlap distance between O and M were considered as shown in Table 1. The critical radii overlap distance of O–K was 1.17 times larger than that of O–Na. This suggests a greater possible overlap between K_9 and O_2 than that between Na_9 and O_6. This was verified and confirmed later by monitoring the respective core and lone pair electron occupancies using NBO analysis. While the bond angle of Si–O–K is narrowly larger than that of Si–O–Na, it is also interesting to note that the non-bonded distance between K_9 and the next neighboring bridging oxygen O_3 is 1.17 times larger than that of Na_9 and O_5. However, the effective way to understand the differences of influence between the cations on the Q^0 species is by studying the extent of delocalization of electrons from the localized electron centres in the molecular structure. The natural bonding orbital (NBO) theory based calculation provides appropriate analysis and the comprehension about the delocalization of electrons in the geometry of M–Q^0 models are discussed here.

4. The NBO analysis

The natural bonding orbital (NBO) analysis was performed extensively on each configuration at every interval of Si–O–M bond angle variation for both Na–Q^0 and K–Q^0. The extent of electron delocalization in terms of the Lewis core, bonding and non-Lewis valence and Rydberg components were analyzed. The electronic occupancies of few components that are directly connected to the central Si atom and which thereby can directly affect the electron density around Si atom are listed in Tables 2 and 3, for Na–Q^0 and K–Q^0, respectively.

The changes in the electronic occupancies of the above components as a function of the Si–O–M bond angle were examined. This helped in understanding the reasons for the changes in the effective core component of central Si atom in both Q^0 species. As mentioned earlier, the changes in the net occupancies of the core of central Si could be directly correlated to the effective NMR chemical shielding of ^{29}Si. In general, during this study, it is observed that the exchanges in the respective occupancies are quite sensitive. They render clear and contrasting distinctions by providing a quantitative picture about the extent of delocalization of the electrons in the system as a whole.

Firstly, the possibilities of characteristic electronic interactions between the cation and the next neighboring (non-bonded) oxygen atoms were analyzed ie., between Na_9 and $O_5(H_8)$ of Na–Q^0 model and K_9 and $O_3(H_4)$ of K–Q^0 model. As seen in Table 2 and 3, the core

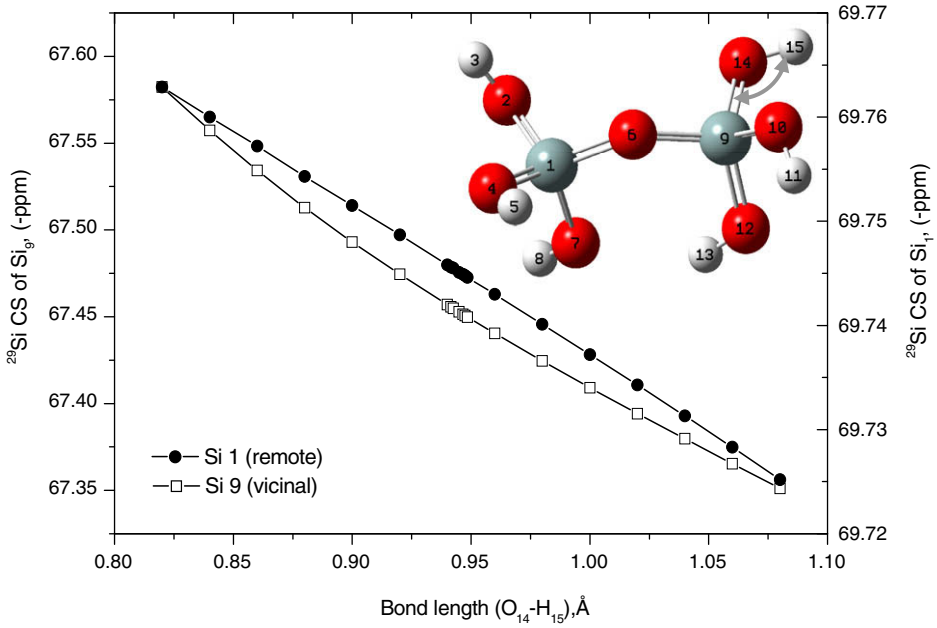

Fig. 5a. Plot of varying ^{29}Si NMR δ of dimeric Q^1 species vs O–H bond length – comparison between the vicinal and remote effects.

of Na_9 constantly increases while that of K_9 initially increases and later gets saturated. The lone pair (LP) and core occupancies of the respective oxygen atoms in each model also vary differently. The LP of O_5 of Na–Q^0 decreases while that of O_3 of K–Q^0 increases. The O_5 core of Na–Q^0 is constant where as the O_3 core of K–Q^0 increases. This shows that in Na–Q^0, there is a significant electron delocalization from O_5 suggesting a strong inter-molecular interaction between Na_9 and O_5. However, in the case of Na–Q^0, the delocalization from O_3 is not significant and on the other way, there seems to be an overall increase in its occupancies. This is the prime distinction observed in the delocalization of electrons with respect to the characteristic interaction of the cation with the neighboring oxygen atoms.

The optimized geometries of both models primitively suggest that one of the strongest modes of interaction could be between the LP of the oxygen and the cation. To study and verify this, the other possible interactions with oxygen were examined using the NBO analysis and it was observed that the most dominating ones are the bonding interaction with terminal H atoms and that with the central Si atom. Since the central Si is secondarily attached with other three oxygen atoms, O–Si interactions were not so sensitive to the changes in electron density around oxygen of our interest. However, the bonding interaction with the terminal H atom was highly sensitive for the changes in LP of the oxygen. This could clearly be monitored through the changes in the O–H Lewis bonding occupancies. In Na–Q^0 the O_5–H_8 bonding occupancy initially increases and later decreases as the LP of O_5 constantly decreases. This change shows that during the bond angle variation the receding Na_9 (from the O_5) is reactively bonded via electron delocalization until it reaches the equilibrium geometry. However, this is not observed for K_9 with O_3 where the O_3–H_4 bond occupancy is constantly increasing. In the case of K–Q^0, both the Si core changes (as shown in Fig. 7) and the Si_1–O_2–K_9 bond angle variations (as shown in Fig. 4) show harmonic trends, proving that the delocalization between K_9 and K–Q^0 is principally through the bonded O_2 atom and not through the non-bonded O_3 atom. This is directly reflected in the NMR chemical shielding values as shown in Fig. 4. This gives a clear picture that the cation–LP_{oxygen} interaction is highly sensitive and characteristic to the cation attached to the Q^0 species.

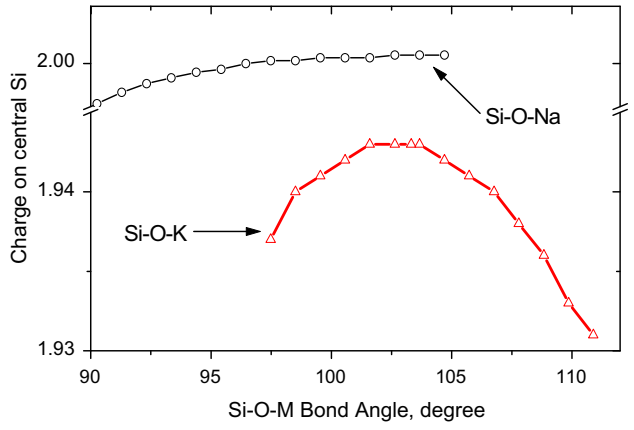

Fig. 5b. Plot of Mulliken charges of Si in Q^0 species with different cations Na^+ and K^+ as a function of the Si–O–M angle.

To confirm the results of NBO analysis, particularly the differential electronic interactions between the cation and non-bonded neighboring oxygen, molecular total electron density cubes were generated through the SCF based energy optimization of both the Q^0 models and the iso-surfaces were mapped at an iso-value of 0.02. Figs. 8a and b show the sliced iso-surfaces of Na and K substituted Q^0, respectively. At iso-value = 0.02, the acute overlapping of the electron density between Na_9 and O_5 is explicitly seen where as it is not observed in the case of K–Q^0. This further confirms the comparatively stronger interaction between the non-bonded O and Na as observed earlier in the NBO analysis. For a comparative case of a model Q^0 with both Na and K (Fig. 1e), the picture of electron density is interestingly different (Fig. 8c). In the case of Na–K–Q^0, it seems there is a relative competition between the two cations, Na and K in the abstraction of electrons from the species. As seen in Fig. 8c, K attracts more electrons while Na becomes more electropositive leading to a higher polarization in the system. This situation explains the earlier experimental report that shows that for certain zeolites, it is possible that an optimum ratio of combination of Na and K selectively reduces the crystallization

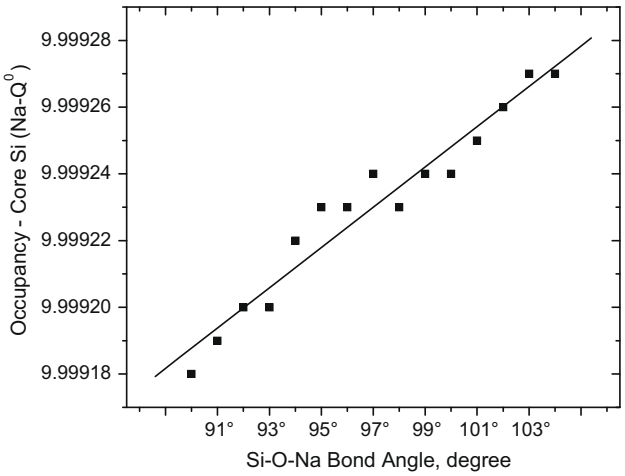

Fig. 6. Fitted plot of the Si–Core electronic occupancy of Na–Q^0.

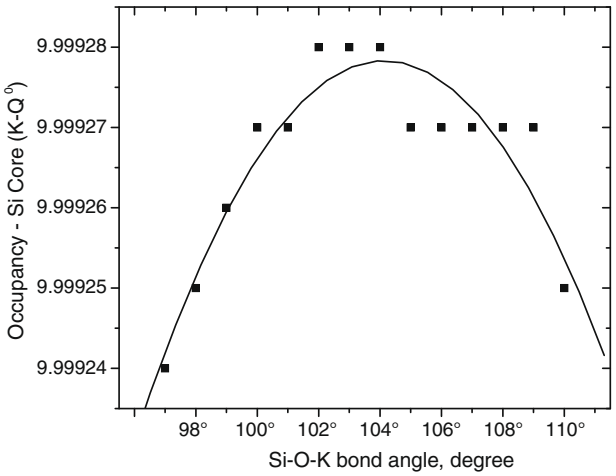

Fig. 7. Fitted plot of the Si–Core electronic occupancy of K–Q^0.

period and enhances the yield [30]. As a consequence of the larger polarization, a dissociative cleavage of O–H bond is spontaneous, yielding anionic Q^0 species, such as $\{MOSi(OH)_2–O^-\}$. Such highly reactive species freely combines with the adjacent Q^0 species surrounding it in the synthesis gel. This facilitates easier oligomerization through ionization of Q^0 species and enhances the yield of crystallization.

We further attempted to perceive a quantitative picture about the differences in the interactions between the LP_{oxygen} and the two mono-valent cations, Na and K using the second order perturbation theory based energy calculations. As described earlier, this provided significant information about the energetics associated with difference types of delocalization in the molecular systems.

5. The perturbation theory based energy analysis

Detailed perturbation theory based energy analysis was performed on all the various geometries used during the process of

Table 2
NBO occupancies of the Na–Q^0 model as a function of $Si_3–O_6–Na_9$ bond angle.

Bond angle	$Si_3–O_6$ Lewis	$Si_3–O_6$ non-Lewis	Si_3 core	O_6 core	O_6 lone pair	Na_9 core	$O_5–H_8$ Lewis	O_5 lone pair	$Si_3–O_5$ Lewis
90°	5.88632	0.29914	**9.99918**	1.99983	**1.97,651**	**9.97130**	1.99344	3.93519	1.93588
91°	5.88747	0.29907	**9.99919**	1.99983	**1.97652**	**9.99736**	1.99346	3.93513	1.93586
92°	5.88859	0.29900	**9.99920**	1.99983	**1.97655**	**9.99756**	1.99348	3.93507	1.93583
93°	5.88968	0.29895	**9.99920**	1.99983	**1.97658**	**9.99773**	1.99349	3.93503	1.93578
94°	5.89075	0.29892	**9.99922**	1.99983	**1.97661**	**9.99787**	1.99349	3.93498	1.93572
95°	5.89180	0.29890	**9.99923**	1.99983	**1.97664**	**9.99800**	1.99349	3.93495	1.93565
96°	5.89280	0.29889	**9.99923**	1.99983	**1.97668**	**9.99811**	1.99349	3.93492	1.93557
97°	5.89379	0.29889	**9.99924**	1.99983	**1.97673**	**9.99821**	1.99348	3.93489	1.93548
98°	5.89488	0.29873	**9.99923**	1.99983	**1.97677**	**9.99829**	1.99347	3.93487	1.93539
99°	5.89582	0.29875	**9.99924**	1.99983	**1.97681**	**9.99836**	1.99346	3.93485	1.93528
100°	5.89673	0.29878	**9.99924**	1.99983	**1.97686**	**9.99841**	1.99344	3.93482	1.93516
101°	5.89761	0.29879	**9.99925**	1.99983	**1.97691**	**9.99846**	1.99342	3.93480	1.93504
102°	5.89849	0.29884	**9.99926**	1.99983	**1.97697**	**9.99850**	1.99340	3.93476	1.93492
103°	5.89932	0.29889	**9.99,927**	1.99983	**1.97702**	**9.99852**	1.99337	3.93470	1.93479
104°	5.90015	0.29897	**9.99927**	1.99983	**1.97708**	**9.99856**	1.99335	3.93465	1.93466

Table 3
NBO occupancies of the K–Q^0 model as a function of $Si_1–O_2–K_9$ bond angle.

Bond angle	$Si_1–O_2$ Lewis	$Si_1–O_2$ non–Lewis	Si_1 core	O_2 core	O_2 lone pair	K_9 core	$O_3–H_4$ Lewis	O_3 lone pair	$Si_1–O_3$ Lewis
97°	5.89004	0.29645	**9.99924**	1.99974	1.97860	17.99420	1.99100	3.92521	1.93844
98°	5.89158	0.29580	**9.99925**	1.99975	1.97858	17.99429	1.99136	3.92682	1.93770
99°	5.89312	0.29514	**9.99926**	1.99976	1.97856	17.99435	1.99171	3.92844	1.93693
100°	5.89341	0.29376	**9.99927**	1.99977	1.97829	17.99436	1.99206	3.93014	1.93617
101°	5.89594	0.29414	**9.99927**	1.99978	1.97846	17.99448	1.99236	3.93145	1.93530
102°	5.89660	0.29264	**9.99928**	1.99979	1.97829	17.99442	1.99270	3.93343	1.93457
103°	5.89882	0.29292	**9.99928**	1.99979	1.97840	17.99452	1.99296	3.93438	1.93357
104°	5.89976	0.29213	**9.99928**	1.99980	1.97827	17.99452	1.99324	3.93598	1.93273
105°	5.90077	0.29150	**9.99927**	1.99981	1.97816	17.99453	1.99352	3.93760	1.93187
106°	5.90185	0.29100	**9.99927**	1.99981	1.97807	17.99455	1.99378	3.93920	1.93102
107°	5.90300	0.29058	**9.99927**	1.99982	1.97798	17.99456	1.99403	3.94079	1.93016
108°	5.90417	0.29021	**9.99927**	1.99982	1.97790	17.99456	1.99427	3.94233	1.92928
109°	5.90529	0.28985	**9.99927**	1.99983	1.97781	17.99456	1.99449	3.94379	1.92839
110°	5.90632	0.28948	**9.99925**	1.99983	1.97772	17.99455	1.99470	3.94517	1.92747

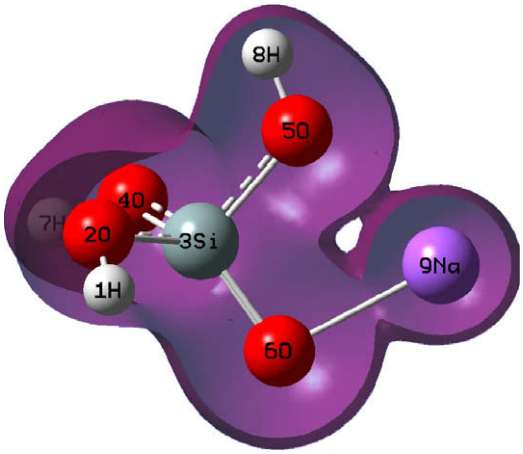

Fig. 8a. Sliced view of electron density iso-surface of optimized Na–Q^0 (isovalue – 0.02).

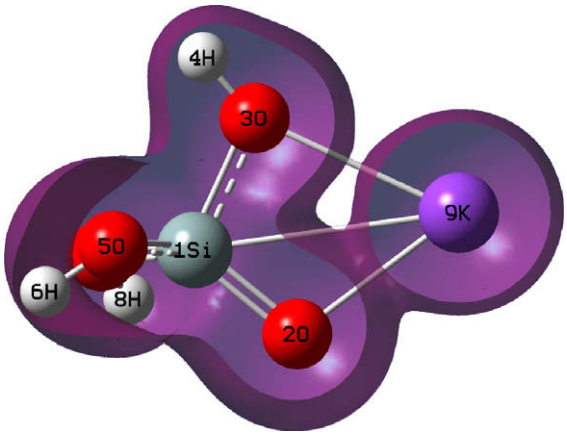

Fig. 8b. Sliced view of electron density iso-surface of optimized K–Q^0 (isovalue – 0.02).

bond angle variations on both Q^0 species followed by the NBO analysis. The stabilization energy due to the electron delocalization from the LP of non-bonded oxygen to the respective cation for three geometries representing the minimum, medium and large Si–O–M angle has been listed in Table 4. Firstly the analysis showed that there is a significant delocalization from the LP of the non-bonded oxygen to the LP and Rydberg orbital of the attached cations. Secondly, the cumulative stabilization energy due to the delocalization from different donor NBOs of oxygen LP to various acceptor NBOs of cation at three different angles as listed shows the changes in the quantum of energy during the variation.

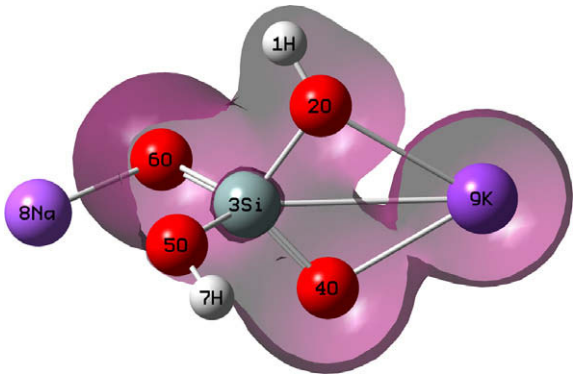

Fig. 8c. Sliced view of electron density iso-surface of optimized Na–K–Q^0 (isovalue – 0.02).

The last column provides the difference in the stabilization energy (δE_s) with in the range of bond angle variation.

It is observed in every case that the energy of stabilization due to delocalization from LP of O_5 to the acceptor NBOs of Na_9 are comparatively larger than that due to delocalization from LP of O_3 to the acceptor NBOs of K_9. The difference in the stabilization energies between the lowest and the highest bond angles during the variation in Na–Q^0 is 4.65 kcal/mol where as that in the case of K–Q^0 is merely 0.5 kcal/mol. This directly proves that the energetics associated with the electron delocalization between Na_9 and O_5 is much higher compared to that between K_9 and O_3 in K–Q^0 model. Hence the results of the energy analysis based on the stabilization due to the electron delocalization are not only in complete correspondence with but further quantitatively support the earlier results based on NBO analysis and electron density mapping as observed in the present report.

6. Conclusions

The influence of local structure of Q^0 silicate precursor species on the ^{29}Si NMR chemical shielding has been investigated using *ab initio* quantum mechanics based DFT calculations. The computed isotropic NMR chemical shift values of different alkali metals such as Na, K and Ca substituted Q^0 species have been shown to be essentially dependent on the local molecular structure around the central Si atom. Furthermore, the studies carried out on an illustrative dimer Q^1 model shows that the influence of the local structure is highly localized and do not perturb the chemical shielding of the remote Si atoms. The changes in the NMR δ values during the Si–O–M bond angle variation carried out on Q^0 species with cations such as Na and K show that the change in the local structure of Q^0 species is found to be truly characteristic of nature of cation attached. The extensive NBO analysis provides help in comprehending the various reasons for the changes in the effective core of the

Table 4
Stabilization energy due to delocalization from LP of oxygen to the alkali cation.

Alkali cation (Q^0)	Donor NBOs (i)	Acceptor NBOs (j)	Si–O–M bond angle (°)	Total E(2) (kcal/mol)	δE_s[a] (kcal/mol)
Na	LP–O_5	LP & Ry–Na_9	90	6.67	4.65
			97	4.08	
			104	2.04	
K	LP–O_3	LP & Ry–K_9	97	1.50	0.50
			103	1.32	
			110	1.00	

[a] δE_s – difference in stabilization energy observed during the Si–O–M bond angle variation with in the respective angle range as given above; LP – lone pair; Ry – Rydberg orbital.

central Si atom of Q^0 species. Through the differences in the variation of electronic occupancies of O–H bonds, NBO studies suggests that there is an apparent distinction between Na and K in terms of their interactions with the lone pair electrons of the neighboring non-bonded oxygen atom. Observing the NBO results based on the electronic occupancies of Si core and the corresponding calculated ^{29}Si NMR δ values, it is apparent that the NMR δ is highly sensitive to the exchanges associated with the core occupancies of central Si atom. The electron density iso-surface maps generated from the density cubes gave direct evidence for the fact that Na interacts more strongly than K with the Q^0 species which were in consistent with results of the NBO and the computed NMR chemical shifts. When both Na and K cations are present, the results show that the Q^0 species is highly polarized leading to easier ionization and facile crystallization. Hence, as reported earlier [30], an optimized ratio of both Na and K thus enhances the zeolite crystallization and yield. Perturbation theory based energy analysis further provided a quantitative picture about the different intensities of delocalization of electrons due to Na and K and further confirmed the earlier results.

Acknowledgments

Prof. B. Viswanathan, National Centre for Catalysis Research, IIT-Madras has been acknowledged for access to computational facility/Gaussian package. We would like to acknowledge Dr. Sailaja Krishnamurty, Central Electrochemical Research Institute, Karaikudi for comments and scientific criticisms.

References

[1] C.S. Cundy, P.A. Cox, Chem. Rev. 103 (2003) 663.
[2] M.E. Davis, R.F. Lobo, Chem. Mater. 4 (1992) 756.
[3] R.W. Thompson, in: H.G. Karge, J. Weitkamp (Eds.), Molecular Sieves, vol. 1, Springer-Verlag, Berlin, 1998, p. 1.
[4] J.-L. Guth, H. Kessler, in: J. Weitkamp, L. Puppe (Eds.), Catalysis and Zeolites, Springer-Verlag, Berlin, 1999, p. 1.
[5] D.P. Serrano, R. van Grieken, J. Mater. Chem. 11 (2001) 2391.
[6] K.J. Balkus, Progr. Inorg. Chem. 50 (2001) 217.
[7] K. Nishi, R.W. Thompson, in: F. Schuth, K.S.W. Sing, J. Weitkamp (Eds.), Handbook of Porous Solids, vol. 2, Wiley-VCH, Weinheim, 2002, p. 736.
[8] A. Corma, in: E. van Steen, L.H. Callanan, M. Claeys (Eds.), Proc. 4th Int. Zeolite Conf., Catal. Soc. S. Africa, Cape Town, 2004, p. 25.
[9] A. Corma, M.E. Davis, Chem. Phys. Chem. 5 (2004) 304.
[10] S.P. Zhdanov, in: E.M. Flanigen, L.B. Sand (Eds.), Molecular Sieve Zeolites—I, ACS Adv. Chem. Ser., vol. 101, 1971, p. 20.
[11] S. Mintova, N.H. Olson, V. Valtchev, T. Bein, Science 283 (1999) 958.
[12] C.S. Cundy, P.A. Cox, Micropor. Mesopor. Mater. 82 (2005) 1–78.
[13] R.M. Barrer, Hydrothermal Chemistry of Zeolites, Academic Press, London, 1982 (p. 133).
[14] R.W. Thompson, in: C.R.A. Catlow, R. Vetrivel (Eds.), Modelling and Reactivity in Zeolites, Academic Press, London, 1992, p. 231.
[15] D.W. Breck, Zeolite Molecular Sieves;, Wiley, New York, 1974 (p. 431).
[16a] R. Szostak, Molecular Sieves: Principles of Synthesis and Identification, Van Nostrand Reinhold, New York, 1989. p. 73.
[16b] U.D. Joshi, P.N. Joshi, S.S. Tamhankar, V.P. Joshi, B.B. Idage, V.V. Joshi, V.P. Shiralkar, Thermochimica Acta 387 (2) (2002) 121–130.
[16c] M.N. Johnson, G. Sankar, C.R.A. Catlow, D. O'Connor, P. Barnes, D. Price, Studies in Surface Science and Catalysis 135 (2001) 19–24 (Zeolites and Mesoporous Materials at the Dawn of the 21st Century).
[16d] Chatterjee, F. Mizukami, Chem. Phys. Lett. 385 (12) (2004) 20–24.
[17] J. Perez-Pariente, J.A. Martens, P.A. Jacobs, Appl. Catal. 31 (1987) 35.
[18] J. Perez-Pariente, J.A. Martens, P.A. Jacobs, Zeolites 8 (1988) 46.
[19] A. Erdem, L.B. Sand, J. Catal. 60 (1979) 241.
[20] Z. Gabelica, N. Blom, E.G. Derouane, Appl. Catal. 6 (1983) 227.
[21] L. Moudafi, P. Massiani, F. Fajula, F. Figueras, Zeolites 7 (1987) 63.
[22] C. Corminboeuf, Thomas Heine, Jacques Weber, Chem. Phys. Lett. 357 (2002) 1.
[23] Sailaja Krishnamurty, Thomas Heine, Annick Goursot, J. Phys. Chem. B 107 (2003) 5728;
M. Jorge, Scott M. Auerbach, P.A. Monson, J. Am. Chem. Soc. 127 (2005) 14388–14400.
[24] Gaussian 98 (Revision A.1), M.J. Frisch, G.W. Trucks, H.B. Schlegel, G.E. Scuseria, M.A. Robb, J.R. Cheeseman, V.G. Zakrzewski, J.A. Montgomery, R.E. Stratmann, J.C. Burant, S. Dapprich, J.M. Millam, A.D. Daniels, K.N. Kudin, M.C. Strain, O. Farkas, J. Tomasi, V. Barone, M. Cossi, R. Cammi, B. Mennucci, C. Pomelli, C. Adamo, S. Clifford, J. Ochterski, G.A. Petersson, P.Y. Ayala, Q. Cui, K. Morokuma, D.K. Malick, A.D. Rabuck, K. Raghavachari, J.B. Foresman, J. Cioslowski, J.V. Ortiz, B.B. Stefanov, G. Liu, A. Liashenko, P. Piskorz, I. Komaromi, R. Gomperts, R.L. Martin, D.J. Fox, T. Keith, M.A. Al-Laham, C.Y. Peng, A. Nanayakkara, C. Gonzalez, M. Challacombe, P.M.W. Gill, B.G. Johnson, W. Chen, M.W. Wong, J.L. Andres, M. Head-Gordon, E.S. Replogle, J.A. Pople, Gaussian, Inc., Pittsburgh PA, 1998.
[25] Krzysztof Wolinski, James F. Hinton, Peter Pulay, J. Am. Chem. SOC. 112 (1990) 8251–8260.
[26] E.D. Glendening, J.K. Badenhoop, A.E. Reed, J.E. Carpenter, F. Weinhold, NBO 4.0, Theoretical Chemistry Institute, University of Wisconsin-Madison, Wisconsin, 1994.
[27] A.E. Reed, L.A. Curtiss, F. Weinhold, Chem. Rev. 88 (1988) 899–926.
[28] J.P. Foster, F. Weinhold, J. Am. Chem. Soc. 102 (1980) 7211–7218.
[29] G. Engelhardt, D. Michel, ^{29}Si NMR of Silicate Solutions, High resolution solid-state NMR of silicates and zeolites, John Wiley and Sons, 1987 (Chapter 4, p. 75).
[30] M.A. Camblor, J. Perez-Pariente, Zeolites 11 (1991) 202.